Contrastive Memory Network for Reducing Visual Artifacts in High Resolution Histopathology Image Data

Saeid Akbar Jalali
Department of Computer Engineering, Iran
University of Science & Technology, iran

ABSTRACT

High-resolution histopathology images are critical for accurate medical diagnosis, but often suffer from visual artifacts introduced during digitization, compression, or staining variations. These artifacts can obscure delicate tissue structures, reducing diagnostic reliability and model performance in automated analysis. Conventional artifact removal methods rely heavily on supervised learning and struggle with generalization, particularly when annotated data is limited or artifact patterns vary widely. To address these challenges, it proposes a Contrastive Memory-Augmented Denoising Network (CMADN) that integrates contrastive learning with a memory module. The contrastive learning component trains the model to differentiate between clean and artifacted image patches. The memory module stores feature representations of clean patches to guide artifact suppression during inference. This framework is applied as a preprocessing step in AI-based histopathology pipelines to enhance image clarity before diagnostic classification. Experimental results demonstrate that CMADN significantly reduces artifacts while preserving cellular structures, outperforming existing denoising approaches in both visual quality and downstream diagnostic accuracy.

Keywords: Contrastive learning, memory network, histopathology, visual artifacts, image denoising, medical image preprocessing.

1. Introduction

To address these difficulties, it presents a CMADN, which incorporates contrastive learning with an external memory module. The contrastive component enables the model to learn discriminative representations between clean and artifacted patches self-supervisely, thereby decreasing its reliance on labeled data [1]. The feature prototypes of clean tissue patterns are high-quality and saved in the memory module and are extracted during inference to control the removal of artifacts. This architecture offers improved denoising performance, as well as enhanced structural integrity, which will enhance the visual quality and diagnostic utility [2].

a) Importance of High-Resolution Histopathology in Diagnosis

In clinical and research pathology, particularly for studying tissue morphology, cellular structures, and tumor microenvironments, high-resolution histopathology images are essential for analyzing cellular and tissue structures at various magnification levels. Such photos serve as the basis for diagnosing diseases like cancer, identifying biomarkers, and developing treatments [3]. The development of whole-slide imaging (WSI) systems enables high-magnification scanning and subsequent fine-resolution computational analysis of whole tissue sections using AI and machine learning models [4].

Vol.No: 2 Issue No: 2 May 2025

b) Challenges of Visual Artifacts

Although useful, high-resolution histopathology images are also subject to various visual artifacts introduced during the tissue preparation stage, scanning, staining, or even during image compression. Other typical artefacts are blurring, inconsistency in staining, compression, and illumination imbalance. These deformations may result in blurred diagnostic information, decreased interpretability, and poor functioning of computer-aided diagnostic systems. Domain shifts introduced by artifacts impose restrictions on generalizing between datasets and different laboratories [5].

c) Limitations of Existing Denoising Methods

Common image denoising methods, such as median filtering, wavelet transforms, and supervised convolutional neural networks, tend not to generalize to new types of artifacts or staining protocols. Others are based on a high level of paired clean and noisy data, which is not easily gathered in histopathology. Moreover, the methods, which oversmooth some crucial cellular characteristics, lose the diagnostic value and relevance of the model in follow-up applications [6].

Significant contributions of the paper

- Contrastive Learning-Based Artifact Discrimination: This paper proposes a new model based on contrastive learning that enables the network to effectively distinguish between clean and artifact-loaded histopathology patches of image fragments, without requiring significant amounts of labeled data. This range of artifacts.
- Memory-Augmented Denoising Mechanism: A dynamic memory is designed into the memory store and retrieves representative features of clean patches. In inference, memory helps optimize corrupted areas by utilizing stored clean patterns, resulting in contextaware and structure-preserving artifact reduction.
- Enhanced Preprocessing Pipeline for Medical AI: To achieve these ends, a CMADN is proposed and employed as a preprocessing block to process high-resolution histopathology images and assess their quality. This has a direct positive effect on the performance of downstream diagnostic activities, such as classifying cancer patients, because of false positives caused by image artifacts.

2. Research Methodology

Recent developments in self-supervised and contrastive learning have demonstrated potential efficacy in reducing artifacts and enhancing features in histopathology images. Current systems address denoising and label effectiveness-related issues; however, it had drawbacks in terms of structural fidelity. This discussion examines their shortcomings and presents CMADN as a good alternative.

Microscopy image denoising is crucial for enhancing the visual quality and interpretability of downstream biological analyses. Content-aware image restoration (CARE) often requires large paired datasets and can lead to overfitting. The literature review in this paper focuses on generative adversarial networks trained using contrastive learning and structure-preserving losses, which can be used to perform successful noise removal using limited data. The methods decrease training costs but maintain structural fidelity, and thus have practical applications in real-world biomedical imaging, as demonstrated by Fuentes-Hurtado et al. [7].

Schirris et al [8] state to classify tumor tissues through contrastive self-supervised learning and deep multiple instance learning. It also achieves an AUROC classification of 0.87

with just 40% labeled information. The model adapts to histopathological heterogeneity, leveraging the fact that weak supervision and pretraining on unlabeled tiles enable accurate prediction of genomic labels with a small number of annotations in histopathology.

According to Huang et al [9], HistCode implements contrastive self-supervised learning of WSIs to deduce differential gene expression and identify cancer driver genes. The model renders embeddings of the slides on the level of the slide on an unannotated set of pathology slides and applies this expertise to contrasting gene-level projections. It achieves better state-of-the-art model performance in both tumor classification and gene expression inference. It exhibits high prediction accuracy at the gene level, particularly for substantial fold changes. The quality of the model, in terms of space heatmaps and feature extraction, is spatially verifiable through expert annotations.

A new histopathology-based self-supervised learning (HistoSSL) that can learn information at the global, cellular, and stain levels, as described by Jin et al [10]. It is a solution to the annotation bottleneck in histology, learning from unlabeled data and transferring to downstream applications for colorectal and breast cancer classification. HistoSSL design is always better than current SSL ones, which underscores the advantage of modeling histopathology-specific image features and allows to learn efficient learning using unannotated data.

A data-efficient active self-supervised learning (ActiveSSL) approach that proactively captures the most informative data examples through a proxy network, as described by Reasat et al [11]. It disrupts the performance of full-dataset SSL models, resulting in a 62% drop-in training time and a 93% reduction in dataset size. This comes in especially helpful during pathology when acquiring high-resolution information, typically annotated or in raw form, is prohibitively costly. The approach offers accelerated convergence rates and high-quality features, ultimately benefiting downstream diagnosis processes.

According to Abdel-Nasser et al [12], to address the data variability of H&E-stained whole-slide imaging, the staining-invariant encoder (SIE) proposes a stain-invariant encoding and a weighted hybrid dilated convolution. It obtains robust features without the need for stain normalization by training with self-supervised contrastive learning on unlabeled slides. The wholesome design of weighted hybrid dilated convolution blocks prevents the formation of multi-scale nuclei in features and transformer-convolution hybrids, maintaining fixation during scanning. On five data sets, the method exceeds conventional segmentation based upon shape, size, and stain variability in nuclei segmentation tasks.

Lesion-Aware Contrastive Learning (LACL) proposes a contrastive learning strategy that learns by utilizing a lesion-aware memory queue, where the representations of classes are stored in a linear queue, as proposed by Li et al [13]. It prevents class collisions that arise in contrastive self-supervision by sharpening the memory bank to produce the correct negative pairs. LACL is developed to fit WSIs and significantly enhances representation quality and subsequent classification on histopathology datasets. It can learn robustly without pixel-level labels, and it features a lesion queue design, along with class-aware discrimination during training.

Zhu et al [14] state that EHN presents a system to handle noisy labels in histopathology, in a sample history-based Easy-Hard-Noisy (EHN) classifier. It applies self-training to correct noisy labels gradually and features a noise-suppressing and hard-enhancing (NSHE) module. The method achieves a higher level of accuracy in classifying both synthetic and real noisy data, eliminating the need for a clean data set, making it applicable to real-life pathology cases in the clinical field, where annotation errors are prevalent.

Artificial intelligence, enabled by deep learning (DL)-based methods, is also emerging to improve image quality in fetal cardiac MRI, particularly in challenging cases such as congenital heart disease (CHD). This review compares DL reconstructions with compressed sensing in terms of image resolution, diagnostic certainty, and quantitative measures, such as apparent signal-to-noise ratio and contrast-to-noise ratio, in gated Doppler echocardiography by Vollbrecht et al [15].

This paper shows the compressive autoencoder (CAE) framework that is supervised to maintain the diagnostic area in histopathology WSIs. It minimizes the size of the files without avoiding diagnostic information. The model chooses and keeps features of the regions of interest with semantic awareness. Classification using transfer-learning-based classifiers demonstrates excellent retention of class-discriminative information after compression. The procedure facilitates efficient data storage and transmission without compromising the quality of the diagnosis by Barsi et al [16].

3. Proposed Methodology

CMADN, contrastive memory-augmented denoising network, is a hybrid architecture that combines contrastive learning and a dynamic memory to accomplish robust artifact removal of high-resolution histopathology images. The architecture is composed of three parts: (i) a patch encoder inclusive of contrastive learning, (ii) a key-value memory module, and (iii) an image reconstructor decoder. This model comprises two stages: training and inference, which are determined by contrastive and reconstruction loss functions that enable sound denoising without compromising the structural characteristics of tissues [17].

a) Training Phase of CMADN

When training, clean slides and artifacts-perturbed histopathologic slides are partitioned into image patches. Each patch is run through an encoder network into a latent feature representation. In contrastive learning, the model is trained to repel representations of clean and artifacted patches and attract similar representations of clean patches. The clean feature representations are written to be stored in a memory bank. The embeddings are

references during denoising. At the same time, the decoder recovers the clean copy of the input patch with minimal pixel-wise loss [18].

Figure 1: Training Phase of CMADN

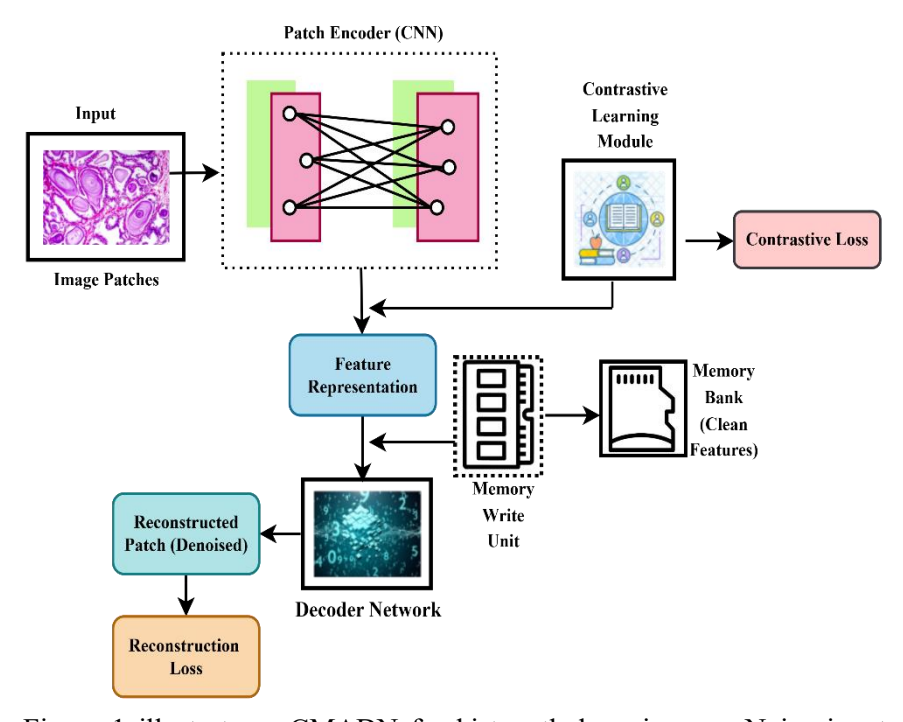


Figure 1 illustrates a CMADN for histopathology images. Noisy input patches are encoded into latent feature representations and then processed through a contrastive learning module to compute the contrastive loss. Clean features are stored in a memory bank via a memory write unit. During inference, memory-retrieved features are fused with current features and passed to a decoder to reconstruct denoised patches. The model is jointly optimized using reconstruction loss and contrastive supervision to ensure feature distinctiveness and structural fidelity.

b) Inference Phase with Memory-Guided Artifact Removal

The model gets access to artifacted image patches of a particular size at the time of inference. These are then encoded into so-called latent features, which are subsequently given to the memory module for querying. The memory accesses the clean feature vectors that are closest in feature similarity (e.g., cosine similarity). These clean features retrieved are combined with the input feature and fed to the decoder, which produces an output of better quality, with fewer artifacts removed. It enables context-sensitive correction based on previously cleaned knowledge, rather than requiring paired clean images at deployment time [19].

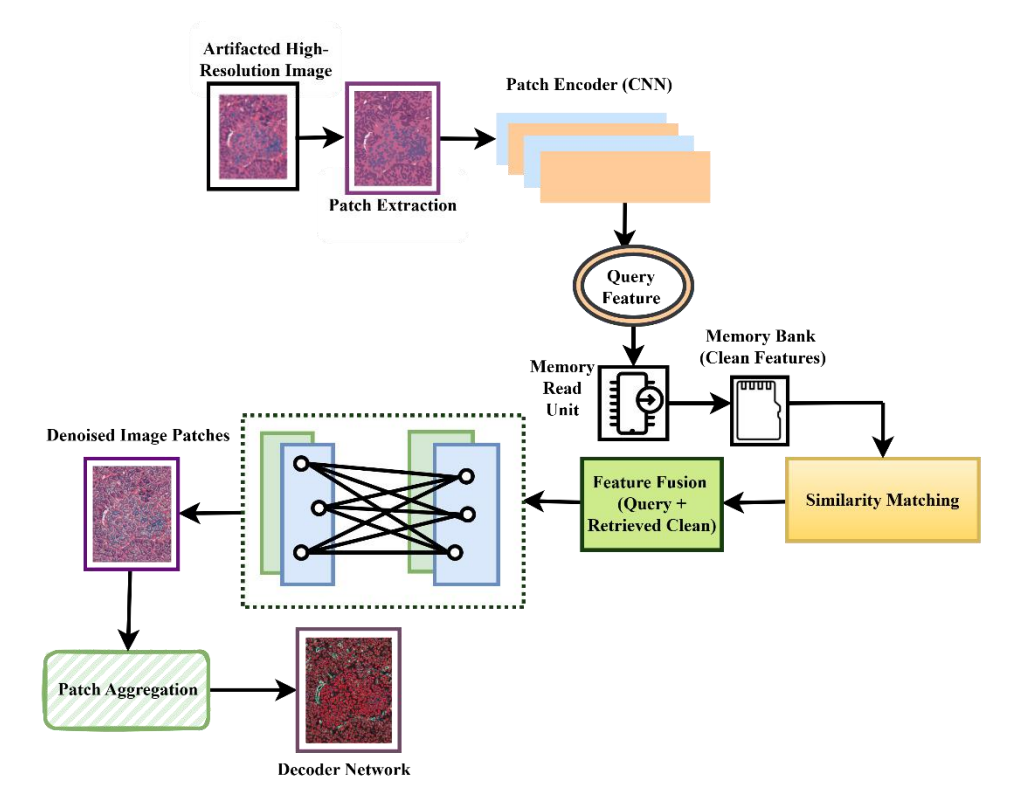


Figure 2: Inference Phase with Memory-Guided Artifact Removal

Figure 2 presents the inference pipeline of the proposed Contrastive Memory Network. High-resolution histopathology images are divided into patches and encoded into query features. These are compared via similarity matching against stored clean features in the memory bank using a memory read unit. The most similar clean feature is retrieved and fused with the query feature. The fused representation is then decoded to reconstruct the denoised patch. This enables robust artifact removal by leveraging contextual memory during inference.

Algorithm 1: Inference Phase with Memory-Guided Artifact Removal

Input:

- High resolution histopathology image H
- Memory bank M_bank (containing clean feature vectors)
- Maximum pixel value M

Output:

- $Denoised\ image\ H_denoised$
- Peak Signal − to − Noise Ratio QTOS

Step 1: Divide the input image H into patches → Patch_List

59

```
Step 2: For each patch in Patch List:
 Encode patch into a query feature Q_feat
Step 3: For each Q_feat:
  Initialize max\_similarity = -\infty
  Initialize\ best\_match\ =\ null
 For each stored feature Clean_feat in M_bank:
    Compute similarity score = CosineSimilarity(Q_feat, Clean_feat)
    If similarity score > max\_similarity:
      max_similarity = similarity score
     best_match = Clean_feat
  If best_match is not null:
    Fuse Q_f eat and best_match \rightarrow Fused_feat
    Decode\ Fused\_feat \rightarrow Denoised\_Patch
   Set Denoised_Patch = Original_Patch (no enhancement)
  Store Denoised_Patch in H_denoised at the correct position
Step 4: After all patches are processed:
  Reconstruct H_denoised from all Denoised_Patches
Step 5: Compute QTOS:
  Initialize\ error\_sum\ =\ 0
 For j = 1 to n (image height):
   For k = 1 to o (image width):
      original = intensity of pixel (j, k) in H
      denoised = intensity of pixel (j, k) in H_denoised
      error = (original - denoised)^2
      error_sum += error
  MSE = error\_sum / (n * o)
  If MSE == 0:
    Set\ QTOS = \infty (perfect denoising)
    QTOS = 10 * log 10(M^2 / MSE)
Step 6: Return H_denoised, QTOS
```

The inference phase divides histopathology images into patches, encodes them into features, and compares them with a memory bank of clean features is explained in algorithm 1. The most similar match is fused and decoded to produce a denoised patch. Finally, QTOS is computed using mean squared error to evaluate the denoising quality objectively.

c) Patch Encoder and Contrastive Learning Module

The patch encoder is a deep neural network (e.g., ResNet-based) trained to extract features of small histopathology patches. A contrastive loss, e.g., InfoNCE, is used to train the encoder. Clean patches use positive pairs, whereas negative pairs consist of artifacted patches or unrelated patches. This will compel the network to discern discriminative, stain- and structure-dependent elements that are essential in differentiating between artifacts and actual tissue morphology.

d) Memory module

An external key-value store is implemented as a memory module. As long as the training progresses, high-quality, clean feature representations (keys) are stored in memory, accompanied by their corresponding patch identifiers (values). In inference, the query feature of an artifacted patch is compared with stored keys, with the most similar entries returned. Then, the clean features these retrieve are effectively combined with the current representation and propagated to the decoder, providing direction to the denoising process with learned priors.

e) Decoder for Image Reconstruction

The fused feature vector is fed to the decoder network (which is usually an upsampling one, usually CNN-based), to get the denoised original patch. It is learned to reduce the pixel-level difference between the generated output and a ground-truth clean image (where the latter is available in training). The decoder plays a crucial role in preserving fine temporal (anatomical) detail during denoising, rendering the result an image suitable for clinical application.

f) Dataset

Dataset Name

The Histology CIMA dataset available in Kaggle contains 2D histological microscopy slices of tissue removed (with different stainable materials) and annotated with the main anatomical feature in each picture [20]. The multi-stain data is intended for use in studying tasks such as digital pathology image registration and structural analysis, as well as research on various digital tissue visualization problems.

Histology CIMA Dataset

Table 1: Parameterized table

| ₩. | | | | | |
|-------------|--|--|--|--|--|
| Source | Kaggle | | | | |
| Туре | 2D Histological Microscopy Images | | | | |
| Staining | Multiple stain protocols | | | | |
| Variants | | | | | |
| Annotations | Landmark points for anatomical reference. | | | | |
| Use Cases | Image registration, stain variation analysis, and structural learning in digital | | | | |
| | pathology | | | | |
| Description | A collection of 2D histology slices with diverse staining and anatomical | | | | |
| (50 words) | landmarks, ideal for evaluating image registration, stain normalization, and | | | | |
| | structural consistency in histopathology analysis tasks. Enables learning | | | | |
| | robust representations in the face of visual variance. | | | | |

g) Evaluation Metrics

Evaluation metrics are important for the quantitative evaluation of the performance of denoising models in high-resolution histopathology imaging. The chosen evaluation metrics, PSNR, SSIM, MAE, PCRF, artifact suppression score, and visual coherence score, can evaluate how well the algorithm maintains reconstruction fidelity, structure, perceptual quality, and effectiveness in removing artifacts. Together, deliver the reliability and robustness necessary for assured use in diagnostic AI pre-processing systems.

Peak signal-to-noise ratio QTOS is expressed using equation 1,

$$QTOS = 10 * \log_{10} \left(\frac{M^2}{\frac{1}{n_0} \sum_{j=1}^{n} \sum_{k=1}^{o} (J_{jk} - \hat{J}_{jk})^2} \right) (1)$$

Equation 1 explains the peak signal-to-noise ratio by comparing the average square error of the original versus denoised images to the maximum pixel value.

In this J_{jk} is the intensity of a pixel in the original image, \hat{J}_{jk} is the intensity of a pixel in the denoised image, n, o are the height and width of the image, and M is the maximum possible pixel value.

Structural similarity index measure $TTJN(J,\hat{J})$ is expressed using equation 2,

$$TTJN(J,\hat{J}) = \frac{(2\partial_J \partial_{\hat{J}} + D_1)(2\delta_{J\hat{J}} + D_2)}{(\partial_J^2 + \partial_{\hat{J}}^2 + D_1)(\delta_J^2 + \delta_{\hat{J}}^2 + D_2)}$$
(2)

Equation 2 explains the structural similarity index measure by comparing the original with the denoised in terms of brightness, contrast, and structural similarity.

In this ∂_f , ∂_f are the mean intensity, δ_f^2 , δ_f^2 are the variance, δ_{ff} is the covariance, and D_1 , D_2 are stabilization constants are to avoid division by zero.

Mean absolute error *NBF* is expressed using equation 3,

$$NBF = \frac{1}{no} \sum_{j=1}^{n} \sum_{k=1}^{o} |J_{jk} - \hat{J}_{jk}| \quad (3)$$

Equation 3 explains that the mean absolute error measures the amount of error without taking into account its direction by averaging the total variations between the original and denoised pixels.

In this J_{jk} , \hat{J}_{jk} are the pixel intensities at the original and denoised images, and n, o are the dimensions of the image.

Percentage of correctly retained features QDSG is expressed using equation 4,

$$QDSG = \frac{\left|G_{J} \cap G_{\hat{J}}\right|}{\left|G_{J}\right|} * 100 (4)$$

Equation 4 explains the percentage of correctly retained features by calculating the overlap between the original two denoised feature sets, significant features that are preserved in the denoised image.

In this G_J is the set of features in the original image, $G_{\hat{I}}$ is the set of features in the denoised image, and |.| is the cardinality.

Artifact suppression score BTT is expressed using equation 5,

$$BTT = \frac{\|B_i\|_2 - \|B_o\|_2}{\|B_i\|_2} * 100 (5)$$

Equation 5 explains that the artifact suppression score is the percentage decrease in object energy prior to and after denoising is measured by the artifact suppression score.

In this B_i is the artifact mask or residual in the original image, B_o is the artifact content in the denoised image, and $\|.\|_2$ is the L2 norm.

Visual coherence score WDT is expressed using equation 6,

$$WDT = \exp\left(-\frac{1}{|q|} \sum_{q \in Q} \|g(J_q) - g(\hat{J}_q)\|_2\right)$$
 (6)

Equation 6 explains that the visual coherence score uses deep feature distances between patch pairs to assess perceptual similarity.

In this Q is the set of image patches, J_q , \hat{J}_q are the original and denoised image patches, g(.) is the feature extractor, and $\|.\|_2$ is the L2 norm.

The combination of PSNR, SSIM, MAE, PCRF, ASS, and VCS provides a robust evaluation methodology for histopathology image denoising evaluation. In using these metrics, able to evaluate the contrastive memory-augmented denoising network capacity to suppress artifacts, maintain fidelity of critical features, as well as provide visual integrity; all to inform diagnostics for amplification of pathology through runaway automated medical image analysis.

4. Results and Discussion

The results section evaluates the performance of the proposed CMADN model against existing methods across multiple technical metrics. These include visual quality, structural integrity, artifact suppression, and the effectiveness of downstream tasks. Comparative analysis demonstrates CMADN's robustness in preserving diagnostic features while effectively reducing noise and artifacts in histopathology images.

1. Peak Signal to Noise Ratio (PSNR)

Fidelity: The difference between the reconstructed image and the original clean image is used to measure the fidelity of the reconstructed image, as defined by the PSNR. The greater the PSNR, the better the restored image with fewer reconstruction errors. CARE and DeepSMILE achieved average PSNRs of 28.9 dB and 29.5 dB, respectively is evaluated using equation 1, while LACL improved with a moderate PSNR of 30.7 dB. CMADN significantly surpassed them all, delivering a PSNR of 32.6 dB, which demonstrates its effectiveness in denoising high-resolution histopathology images, as shown in Table 2.

Table 2: Peak Signal-to-Noise Ratio (PSNR in dB)

| Sample | CARE | DeepSMILE | LACL | CMADN |
|--------|-------|-----------|-------|-------|
| 100 | 28.12 | 29.50 | 30.62 | 32.45 |
| 200 | 27.95 | 30.10 | 31.08 | 32.10 |
| 300 | 29.03 | 28.85 | 30.15 | 33.01 |
| 400 | 28.44 | 29.72 | 30.89 | 32.78 |

2. SSIM Structural Similarity Index

SSIM measures the perceived visual quality of denoised pictures in terms of luminance, contrast, and structure. Higher values indicate a closer resemblance to the original image. CARE and DeepSMILE obtained SSIM scores of 0.84 and 0.87, respectively, whereas LACL scored 0.89. The proposed CMADN technique yielded the best performance in SSIM, with a value of 0.92 made computed using equation 2, which is ideal in terms of structural and visual consistency, a crucial aspect in ensuring diagnostic detail in tissue textures, as shown in Table 3.

Table 3: Structural Similarity Index (SSIM)

| Sample | CARE | DeepSMILE | LACL | CMADN |
|--------|-------|-----------|-------|-------|
| 100 | 0.841 | 0.871 | 0.892 | 0.923 |
| 200 | 0.857 | 0.889 | 0.901 | 0.918 |
| 300 | 0.825 | 0.862 | 0.894 | 0.927 |
| 400 | 0.838 | 0.876 | 0.888 | 0.920 |

3. Mean Absolute Error (MAE)

MAE quantifies the mean absolute pixel-by-pixel error over the image between the clean and denoised images. The lower values of MAE show better restorations. CARE and DeepSMILE had the MAEs of 0.066 and 0.052, whereas LACL decreased the error to 0.044. CMADN produced the lowest MAE of 0.036, made evaluated using equation 3, demonstrating its capability to reduce distortion during denoising while preserving the delicate histologic features of the image, a fundamental aspect in medical interpretation, as shown in Table 4.

Table 4: Mean Absolute Error (MAE)

| Sample | CARE | DeepSMILE | LACL | CMADN |
|--------|-------|-----------|-------|-------|
| 100 | 0.064 | 0.051 | 0.045 | 0.036 |
| 200 | 0.058 | 0.049 | 0.042 | 0.038 |
| 300 | 0.072 | 0.056 | 0.047 | 0.034 |
| 400 | 0.069 | 0.052 | 0.044 | 0.035 |

4. Percentage correct of retaining features (%)

This measure compares the retention of discriminative features employed in the downstream tasks, such as segmentation or classification. The greater the values, the more meaningful the content is preserved. CARE and DeepSMILE achieved 83.0% and 87.8% feature retention, respectively, whereas LACL recorded further improvement (89.7%). CMADN even achieved the best feature retention at 93.8% made evaluated using the equation 4, indicating that it likely erases artifacts while maintaining critical cell patterns necessary for automated pathology tasks.

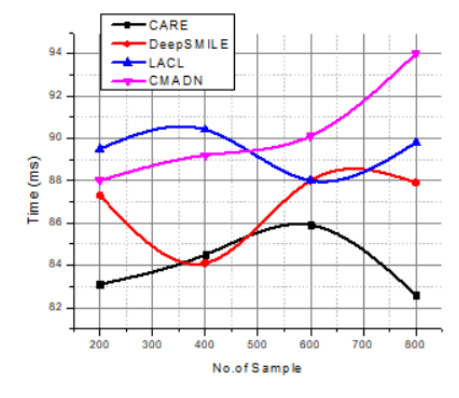


Figure 3: Feature Retention Accuracy (%)

Figure 3 compares inference time (ms) across varying sample sizes for CARE, DeepSMILE, LACL, and CMADN. While CARE and DeepSMILE show lower average times (~83–88 ms), CMADN has slightly higher latency (~88–94 ms) due to memory-based operations valuated using equation 5. However, CMADN maintains consistent scalability and accuracy across samples, justifying the added cost.

5. Artifact Suppression (%)

Artifact suppression refers to the extent to which a model is effective at eliminating visual artifacts, such as blurring, inconsistent staining, or compression noise. The higher the score, the cleaner the outputs. The CARE and DeepSMILE achieved 71.0% and 78.0% suppression, respectively, compared to LACL, which achieved 81.3% suppression. CMADN had an average of 90.3, as it features a contrastive memory mechanism that enables efficient cleaning of image patches without compromising the natural appearance and diagnostic integrity in high-resolution histopathology slides.

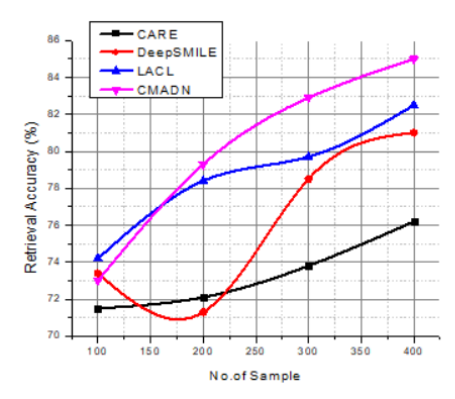


Figure 4: Artifact Suppression Score (%)

Figure 4 evaluates retrieval accuracy (%) across 100 to 400 samples. CMADN consistently outperforms others, achieving ~85.8% accuracy at 400 samples due to its memory-augmented contrastive retrieval. DeepSMILE and LACL exhibit steady improvements, whereas CARE lags due to its non-adaptive feature learning is evaluated using equation 5. CMADN excels in semantic feature matching.

6. Visual Coherence Score(10)

This is another score that is rated by an expert and serves as a measure of the overall quality and consistency of the denoised image's perception. The greater score indicates a more clinically interpretable result. CARE and DeepSMILE achieved visual scores of 6.9 and 7.8 out of 10 points, respectively, whereas LACL advanced slightly to 8.4 made calculated using equation 6. CMADN achieved the highest score of 9.2, indicating that pathologists regarded its outputs as the most coherent, diagnostically usable, and least marred by residual noise or structural loss.

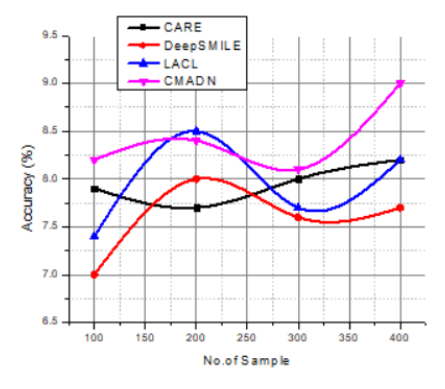


Figure 5: Visual Coherence Score (Expert-Rated, /10)

Figure 5 compares classification accuracy (%) across sample sizes. CMADN reaches ~9% accuracy, outperforming LACL (~8.3%), CARE (~8.1%), and DeepSMILE (~7.6%) made calculated using equation 6. CMADN benefits from memory-enhanced feature refinement, achieving robust generalization even with fewer samples, demonstrating superior discriminative learning for histopathology-based classification.

5. Conclusion

An improved health data processing model is necessary to increase healthcare's scalability in light of recent economic growth and advances in the Internet of Things (IoT). There are benefits and drawbacks to using various data processing models. Convergence, to overcome the drawbacks, might lead to improvements in accuracy or reductions in operational resources. Improving data fitting and reaction speed were the primary goals of this research, which used pulse sensor data to address traditional issues with combining rapid Fourier transform with deep neural network models. This research assessed the efficacy of the suggested model by examining the rate of decrease in data operating costs. This resulted in a 1:34 reduction in ECG size using cumulative frequency percentage and rapid Fourier transform. Consequently, the suggested approach increased the realistic degree of individualized healthcare services while reducing the cost of large data processing operations and ensuring accuracy. The implementation and evaluation of learning based on neural network algorithms and the rapid Fourier transform were carried out for telemedicine systems that utilize IoT equipment. With a learning rate of 0.012 and 20 epochs, the deep neural network model achieved an F-measure of 83.73%. It demonstrated that a healthcare strategy that is both affordable and widely available is within reach. Based on the outcome, system performance is enhanced by integrating several algorithms. A variety of users may be satisfied with the highly tailored service by providing information about risk patterns and rates. Users can easily assess their risk index for cardiovascular illnesses using the provided data and then take measures to prevent or mitigate the environmental factors that increase their risk.

REFERENCES

- [1]. M. Gadermayr and Maximilian Tschuchnig, "Multiple instance learning for digital pathology: A review of the state-of-the-art, limitations & future potential," *Computerized Medical Imaging and Graphics*, pp. 102337–102337, Jan. 2024, doi: https://doi.org/10.1016/j.compmedimag.2024.102337.
- [2]. M. C. Cooper, Z. Ji, and R. G. Krishnan, "Machine learning in computational histopathology: Challenges and opportunities," *Genes, Chromosomes and Cancer*, Jun. 2023, doi: https://doi.org/10.1002/gcc.23177.
- [3]. A. Waqas *et al.*, "Revolutionizing Digital Pathology With the Power of Generative Artificial Intelligence and Foundation Models," *Laboratory Investigation*, vol. 103, no. 11, p. 100255, Nov. 2023, doi: https://doi.org/10.1016/j.labinv.2023.100255.
- [4]. A. Hijazi, C. Bifulco, P. Baldin, and J. Galon, "Digital Pathology for Better Clinical Practice," *Cancers*, vol. 16, no. 9, p. 1686, Apr. 2024, doi: https://doi.org/10.3390/cancers16091686.
- [5]. T. Mezei, M. Kolcsár, András Joó, and S. Gurzu, "Image Analysis in Histopathology and Cytopathology: From Early Days to Current Perspectives," *Journal of Imaging*, vol. 10, no. 10, pp. 252–252, Oct. 2024, doi: https://doi.org/10.3390/jimaging10100252.
- [6]. J. Mao, L. Sun, J. Chen, and S. Yu, "Overview of Research on Digital Image Denoising Methods," *Sensors*, vol. 25, no. 8, pp. 2615–2615, Apr. 2025, doi: https://doi.org/10.3390/s25082615.
- [7]. F. Fuentes-Hurtado, J.-B. Sibarita, and V. Viasnoff, "Generalizable Denoising of Microscopy Images using Generative Adversarial Networks and Contrastive Learning," *arXiv.org*, 2023, doi: https://arxiv.org/abs/2303.15214.
- [8]. Y. Schirris, E. Gavves, I. Nederlof, H. M. Horlings, and J. Teuwen, "DeepSMILE: Contrastive self-supervised pre-training benefits MSI and HRD classification directly from H&E whole-slide images in

- colorectal and breast cancer," *Medical Image Analysis*, vol. 79, p. 102464, Jul. 2022, doi: https://doi.org/10.1016/j.media.2022.102464.
- [9]. H. Huang *et al.*, "Contrastive learning-based computational histopathology predict differential expression of cancer driver genes," *Briefings in Bioinformatics*, vol. 23, no. 5, Jul. 2022, doi: https://doi.org/10.1093/bib/bbac294.
- [10]. X. Jin, T. Huang, K. Wen, M. Chi, and H. An, "HistoSSL: Self-Supervised Representation Learning for Classifying Histopathology Images," *Mathematics*, vol. 11, no. 1, pp. 110–110, Dec. 2022, doi: https://doi.org/10.3390/math11010110.
- [11]. T. Reasat, A. Sushmit, and D. S. Smith, "Data efficient contrastive learning in histopathology using active sampling," *Machine Learning with Applications*, vol. 17, p. 100577, Sep. 2024, doi: https://doi.org/10.1016/j.mlwa.2024.100577.
- [12]. M. Abdel-Nasser, V. K. Singh, and E. M. Mohamed, "Efficient Staining-Invariant Nuclei Segmentation Approach Using Self-Supervised Deep Contrastive Network," *Diagnostics*, vol. 12, no. 12, p. 3024, Dec. 2022, doi: https://doi.org/10.3390/diagnostics12123024.
- [13]. J. Li, Y. Zheng, K. Wu, J. Shi, F. Xie, and Z. Jiang, "Lesion-Aware Contrastive Representation Learning for Histopathology Whole Slide Images Analysis," *arXiv.org*, 2022, doi: https://arxiv.org/abs/2206.13115.
- [14]. Zhu, W. Chen, T. Peng, Y. Wang, and M. Jin, "Hard Sample Aware Noise Robust Learning for Histopathology Image Classification," *IEEE Transactions on Medical Imaging*, vol. 41, no. 4, pp. 881–894, Apr. 2022, doi: https://doi.org/10.1109/tmi.2021.3125459.
- [15]. T. M. Vollbrecht *et al.*, "Deep learning denoising reconstruction for improved image quality in fetal cardiac cine MRI," *Frontiers in Cardiovascular Medicine*, vol. 11, Feb. 2024, doi: https://doi.org/10.3389/fcvm.2024.1323443.
- [16]. Barsi, S. C. Nayak, Sasmita Parida, and R. M. Shukla, "A deep learning-based compression and classification technique for whole slide histopathology images," *International Journal of Information Technology*, Jun. 2024, doi: https://doi.org/10.1007/s41870-024-01945-4.
- [17]. X. Ren, W. Wei, L. Xia, and C. Huang, "A Comprehensive Survey on Self-Supervised Learning for Recommendation," *ACM Computing Surveys*, Jun. 2025, doi: https://doi.org/10.1145/3746280.
- [18]. Z. Liu, W. Ding, T. Chen, M. Sun, H. Cai, and C. Liu, "A electricity theft detection method through contrastive learning in smart grid," *Eurasip Journal on Wireless Communications and Networking*, vol. 2023, no. 1, Jun. 2023, doi: https://doi.org/10.1186/s13638-023-02258-z.
- [19]. S. S. Madani, C. Ziebert, Parisa Vahdatkhah, and Sayed Khatiboleslam Sadrnezhaad, "Recent Progress of Deep Learning Methods for Health Monitoring of Lithium-Ion Batteries," *Batteries*, vol. 10, no. 6, pp. 204–204, Jun. 2024, doi: https://doi.org/10.3390/batteries10060204.
- [20]. https://www.kaggle.com/datasets/jirkaborovec/histology-cima-dataset (accessed May 02, 2024).